

# Development and Validation of a Vehicle Corner Test Rig Designed for Hardware-in-the-Loop Testing

Paulius Kojis<sup>1</sup><sup>a</sup>, Viktor Skrickij<sup>2</sup><sup>b</sup>, Valentin Ivanov<sup>3</sup><sup>c</sup>, Eldar Šabanović<sup>2</sup><sup>d</sup>,  
Marijonas Bogdevičius<sup>1</sup><sup>e</sup> and Tomas Grikenis<sup>1</sup><sup>f</sup>

<sup>1</sup>*Department of Mobile Machinery and Railway Transport, Faculty of Transport Engineering, Vilnius Gediminas Technical University, 10105 Vilnius, Lithuania*

<sup>2</sup>*Transport and Logistics Competence Centre, Faculty of Transport Engineering, Vilnius Gediminas Technical University, 10223 Vilnius, Lithuania*

<sup>3</sup>*Smart Vehicle Systems—Working Group, Technische Universität Ilmenau, Ehrenbergstr, 29, 98693 Ilmenau, Germany*

**Keywords:** Vehicle Corner, Test Rig, Hardware-in-the-Loop, Electric Vehicle, Tyre Forces.

**Abstract:** Many original equipment manufacturers and Tier 1 suppliers have recently proposed various vehicle corner concepts. This technology offers numerous benefits for enhancing vehicle dynamics but presents several challenges. Field testing of the corners installed on a vehicle demonstrator could be an ideal solution to address these challenges. Nevertheless, the proof-of-concept development phase also requires studies on the component and system levels. In this regard, a vehicle corner test rig designed for hardware-in-the-loop testing provides a balanced alternative that combines the accuracy, complexity, and accessibility of experimental works. Real suspension components, including a rotating wheel with tyre, provide realistic suspension kinematics and compliance that are very similar to those experienced in real driving scenarios. However, this approach has limitations because the tyre contact forces and loading conditions cannot be fully replicated in a laboratory environment. This paper explores these aspects and describes a developed comprehensive methodology for eliminating inaccuracies, with results validated accordingly.

## 1 INTRODUCTION

Modern electric vehicle (EV) architectures with individual corner actuators enable new motion control technologies (Armengaud et al., 2021; Cheng et al., 2024). Coupled with an integrated chassis control (ICC) approach, the full potential of multi-actuated vehicles can be exploited, with the benefits of vehicle safety, comfort, fail-safe operation, and redundancy (Skrickij et al., 2024). However, this complex integration requires advanced components and thorough testing. For this reason, automotive researchers and engineers apply various hardware-in-

the-loop (HIL) setups to facilitate testing in real-time (Heydrich et al., 2022; Ivanov et al., 2019).

A corner-based chassis architecture is a potential pathway for further development of EVs. Such architecture typically incorporates in-wheel motors (IWM), brake-by-wire, and steer-by-wire systems; some corners may also feature toe and camber actuators. While the first prototypes of this technology emerged over two decades ago, research and development in this area have gained significant momentum in recent years. Notable contributions come from several Horizon projects, including OWHEEL, SmartCorners, and industrial companies

<sup>a</sup> <https://orcid.org/0000-0003-0566-559X>

<sup>b</sup> <https://orcid.org/0000-0002-8080-875X>

<sup>c</sup> <https://orcid.org/0000-0001-7252-7184>

<sup>d</sup> <https://orcid.org/0000-0002-4724-0787>

<sup>e</sup> <https://orcid.org/0000-0003-4947-7638>

<sup>f</sup> <https://orcid.org/0009-0002-5400-9150>

such as Continental and Hyundai Mobis (Nguyen and Trovão 2024; Kojis et al., 2022).

Novel corner architecture offers numerous advantages. First, it enables torque control at each vehicle corner and torque vectoring that enhances manoeuvrability and stability (Guo et al. 2019; Hori 2004; Jneid and Harth 2024). Additionally, the modular design of vehicle corners facilitates the development of flexible vehicle platforms. Eliminating components such as driveshafts and differentials reduces energy losses and improves vehicle packaging (Deepak et al., 2023). However, there are drawbacks: increased unsprung mass (UM) due to IWM and other components result in comfort and handling issues if passive suspension components are used; larger vehicle inertia around the vertical axis impairs with vehicle stability; increased system complexity, number of parts and price (Kojis et al., 2022).

In order to fully exploit vehicle corners, advanced components and thorough testing are inevitable. Testing can typically be carried out in three main ways: simulation environments, laboratories, and proving grounds, each with its advantages and disadvantages.

Simulations provide high repeatability and rapid evaluation, making them the most cost-effective method for investigating complex systems. However, they can be limited by assumptions that may reduce the accuracy and fidelity of system replication. In addition, the high nonlinearity of certain system elements can make mathematical modelling complex and computationally intensive.

Vehicle field testing on a proving ground can be considered the best option despite being subject to various uncertainties and issues with repeatability. To ensure consistent replicability of tests, vehicle control inputs must remain stable and free from human error.

Laboratory testing serves as a primary alternative to the field testing, offering high repeatability and accelerating the execution of tests. Experiments in the laboratory conditions can be conducted at the whole vehicle level for tasks such as suspension testing, kinematics and compliance (KnC), component durability assessments, ride comfort evaluations, and noise, vibration, and harshness (NVH) testing (Chindamo et al., 2017; Gräbe et al., 2020).

The second group of testing equipment consists of various quarter-car test rigs, categorised into three types according to the literature (Maher and Young, 2010). The first category includes setups that consist solely of a sprung mass (SM), UM, damper, and spring. This configuration is primarily utilised for developing and validating active and semi-active

suspension control systems (Omar et al., 2017; Gysen et al., 2010). The second type incorporates complete suspension components, a wheel and a tyre. Including these elements ensures a more realistic suspension response to vertical excitations induced by the shaker system beneath the tyre (Yu et al., 2019; Lauwerys et al., 2005). This setup can be employed for suspension KnC testing, examining the influence of the tyre on vertical vehicle dynamics, conducting frequency analyses, and prototyping suspension components. The final group features a rolling road, which can be implemented using flat belts or drums. Such construction enables the consideration of brake- and acceleration-induced longitudinal forces, steering-induced lateral forces and associated suspension deflections. Vertical excitation is provided by cleats attached to the rotating surface or by shaking the entire rotating assembly using an eccentric and various actuators (Li and Lee, 2019; Gießler et al., 2022).

Each of the described quarter-car test rigs has inherent flaws and simplifications that can affect the accuracy of the measured quantities and their correlation to field tests. These setups typically allow the SM to move only vertically, meaning they do not account for weight transfer due to braking or acceleration nor capture roll or pitch angles. Flat belt systems tend to produce lower rolling resistance values than observed during field tests, as the belt heats up more and generates higher temperatures on the tyre surface. According to the SAE J 1106 standard, flat belts can induce lateral tyre forces up to 10% greater than those observed with drum-type systems.

On the other hand, drum-type rolling roads can distort the tyre/road contact patch, reducing tyre lateral force and aligning torque while increasing tyre rolling resistance. It is therefore necessary to properly recalibrate the values recorded on corner test rigs to allow comparison with field test results. To address these challenges, automotive researchers and engineers utilise HIL setups (Heydrich et al., 2022; Ivanov et al., 2019; Stolte et al., 2023). In a HIL setup, a mathematical model is connected to a physical system, enabling the investigation of a subsystem under development by incorporating its physical components into a closed-loop mathematical simulation of the overall system (Fathy et al., 2006). In this context, recalculation of physical outputs from the corner test rig is essential to ensure that they align with the expected values from the real system.

The development of HIL systems for vehicle corner testing offers several key benefits (Mihalič et al., 2022): real-time feedback, cost-effectiveness,

scalability and reproducibility. Traditional HIL applications typically involve a single test rig implementation (e.g., brakes, suspension, steering, etc.). However, multiple test rigs in the same laboratory can be interconnected to create a Test-rig-in-the-Loop (TRIL) system (Augsburg et al., 2011). When test setups are distributed between different locations, shared and connected X-in-the-Loop (XIL) testing procedures can be employed (Ivanov et al., 2019).

The literature review indicates that the HIL approach is effective for investigating vehicle corner proof of concept when field testing is not feasible. A new vehicle corner test rig concept has been developed in this regard. The primary contribution of this paper is a detailed methodology for validating developed test rig, aiming to address the key limitations associated with such equipment.

The paper is structured as follows: Section 2 outlines the HIL design for vehicle corner testing. Section 3 identifies the main sources of inaccuracies and discusses strategies for their mitigation, along with the presentation of validation results. Section 4 includes a case study related to vehicle corner HIL testing. Finally, Section 5 summarises the findings and offers an outlook on potential next steps.

## 2 HIL FOR VEHICLE CORNER TESTING

An experimentally validated, sport utility vehicle’s (SUV) mathematical model which is running on the real-time target machine and connected with the corner test rig is used for the HIL application. Vehicle model features 14 degrees of freedom (DoF) and is implemented via the IPG CarMaker and Simulink conjunction. More information regarding the mathematical model can be found in an article by Šabanović et al., 2021. Physical nonlinear corner components, which are hard to model, are used on the corner test rig. The whole system architecture is presented in Figure 1, and the main technical data is presented in Table 1.

Host PC containing the MATLAB and IPG CarMaker HIL software packages is directly connected to the dSPACE real-time target machine. Once the real-time simulation is initialised, the dSPACE ControlDesk is utilised to exchange data between software and hardware components installed on the test rig.

The dSPACE inputs are employed to measure the characteristics and critical values induced by the

experiments on the quarter-car test rig. The wheel transducer measures tyre forces ( $F_x, F_y, F_z$ ) and torques ( $M_x, M_y, M_z$ ). It also provides the angular velocity of the wheel ( $\omega_{wheel}$ ). This velocity is then compared to the reading of the encoder attached to the steel drum ( $\omega_{drum}$ ) axis of rotation, and the longitudinal slip is calculated. Displacement of the actuators is measured by linear potentiometers and supplied to the real-time target machine ( $\alpha_{meas}$ ). Additionally, to implement suspension control, SM and UM vertical accelerations ( $A_{z_{SM}}, A_{z_{UM}}$ ), suspension stroke ( $z_{SM} - z_{UM}$ ) and actual current at the damper valve ( $I_{CES_{meas}}$ ) are measured. The dSPACE outputs are mainly used to send inputs to the low-level controllers of electric toe actuators ( $\alpha, v_\alpha$ ), suspension damper ( $I_{CES_{req}}$ ) and electric motor ( $V$ ) controllers. Since hardware components are installed on the test rig, this HIL setup allows the test of control algorithms, element activation delays, actuators dynamics and overall system operation.

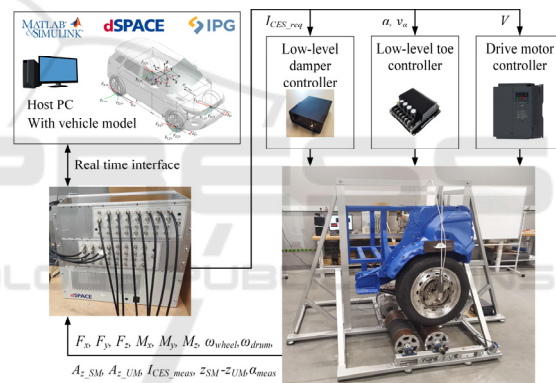


Figure 1: HIL setup.

Such a system has two main drawbacks. First, these setups do not consider vehicle’s roll and pitch angles. As a result, the vertical load does not fully correspond to real-world system dynamics during cornering and braking. For this reason, weight transfer from the simulation environment is applied to recalculate vertical loading in different driving scenarios. Second, contact forces between the tyre and the drum do not represent the actual ones generated in the contact between the road and the tyre in real conditions. Hence, tyre forces and moments generated on the test rig are registered using a wheel force transducer and further recalculated using provided methodology.

Table 1: Vehicle corner test rig specifications.

Parameter	Value
Overall dimensions of test rig (L x W x H)	2.7 x 1.7 x 1.8 m
Minimal sprung mass	200 kg
Maximal sprung mass	900 kg
Electric motor-rated power on drum	11 kW (400 V)
Maximum wheel's linear velocity	170 km/h
Diameter of the drum	0.22 m
Single-toe actuator-rated force	1000 N (12 V 4.6 A)
Rear toe actual range	$\pm 3^\circ$
Controller for the toe actuators	Cytron MDDS30
Vertical actuator	Custom-made semi-active damper with continuously controlled valve
Controller for the vertical actuator	Custom-made low-level damper controller
Wheel force transducer	Michigan Scientific Corporation LW12.8-50
Real-time target machine	dSPACE ds1006 total 64 input and output slots
Software	MATLAB, Simulink, IPG CarMaker HIL, dSPACE ControlDesk
Vertical excitation	Sinusoidal – Amplitude up to 16 mm
Other	Possibility to run drum and belt setups, for IWM consideration, an additional 35 kg mass can be added to UM

### 3 TYRE FORCES RECALCULATION

In typical test rigs with a rolling drum, the maximal longitudinal tyre force is achieved at slip values of around 0.1. However, in such test rigs, the drum diameter is much higher compared to the tyre diameter. In the case under investigation, such construction was not feasible; the drum diameter was only 0.22 m. The registered values must be recalculated since the rolling drum surface has friction and geometrical properties different from the actual road surface. Using such an approach, various road conditions can be simulated (for example, dry/wet asphalt, icy roads, etc.) (Arosio et al., 2005).

A series of braking tests using the vehicle corner test rig have been performed for longitudinal contact force estimation. The wheel was rolling on the steel drum in all of the tests. Different vertical loading scenarios need to be investigated. Mathematical modelling showed that vertical load may change in a wide range from 2000 N to 9000 N. The magnitude of the vertical load during the experiments was solely based on the additional SM. At the beginning of each test run, static load, tyre surface temperature and vehicle suspension settings were registered. Afterwards, the wheel is excited to reach predefined linear velocities of 50 km/h, 75 km/h and 100 km/h. Once the speed has settled in, the braking is applied till the full stop of the wheel. With each load and velocity setting, five tests are performed. The average of the results from 5 braking tests, captured on the same  $F_z$  and wheel linear velocities, are taken to form longitudinal tyre force curves versus slip angle, considering different road types and tyre wear. To omit outliers, data from the force transducer was filtered using median filters. Experimental data showed that maximal longitudinal force is achieved when the slip exceeds 0.2. As described above, the resulting forces must be validated since the tyre contact properties are distorted. For this reason, the actual values of the tyre forces in the longitudinal direction are used, which were generated with the experimentally validated MF 6.1 tyre model at the same slip angles and vertical loads.

These target curves are then divided by the curves gathered in experiments on the test rig with a steel drum. The result of curve division produces longitudinal tyre force recalculation coefficients, and the polynomial curve fit is done to capture the trend of the recalculation coefficients (Figure 2).

In Figure 2, each curve is marked for the specific vertical load and vehicle travel speed, which is 100 km/h. Due to repetition, this paper does not provide results achieved at other loading conditions and velocities.

During the investigation, it was found that a polynomial curve of the fifth order can be used for force recalculation. For all the cases, the value of the determination coefficient was higher than 0.98. Once the database containing polynomial curves is completed for the most common loading scenarios on the test rig, the longitudinal slip, vertical load, and measured longitudinal force proceed to the algorithm, which contains polynomials, and the recalculation is performed. The force recalculation for dry/wet and new/worn tyres using the algorithm proposed above is shown in Figure 3.

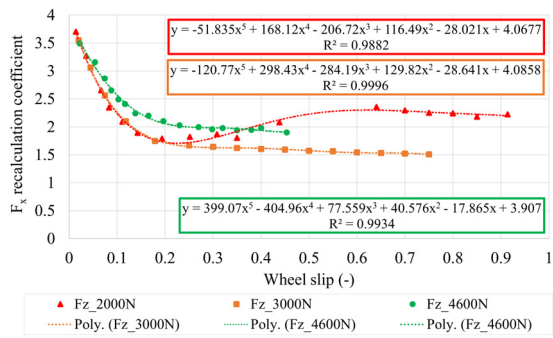


Figure 2: Examples of longitudinal tyre force recalculation coefficients for a few loading cases and velocity 100 km/h.

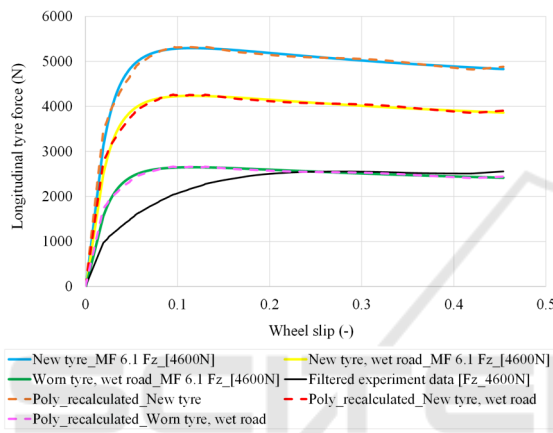


Figure 3: Longitudinal tyre force recalculation for medium vertical loading scenario (4600 N).

Similar conditions were maintained in dedicated experiments for lateral tyre force measurements. Sideslip angle input was generated in the form of an active toe. Due to the used vehicle rear suspension and overall corner construction application, toe amplitude of  $6^\circ (\pm 3^\circ)$  was used. All the required variables for validation were gathered in real-time and saved in the database. The polynomial curves of the fifth order were used for recalculation (Figure 4); for all the cases, the value of the determination coefficient was higher than 0.98.

Since the wheel was cambered due to high vertical load, different polynomial curves were required to capture the asymmetry of the lateral tyre force (Figure 4). Using the same methodology, actual lateral force values were achieved and compared to measurement ones on the test rig. An example of a few scenarios is shown in Figure 5.

For all cases under investigation, the created recalculation methodology matches both longitudinal and lateral forces well.

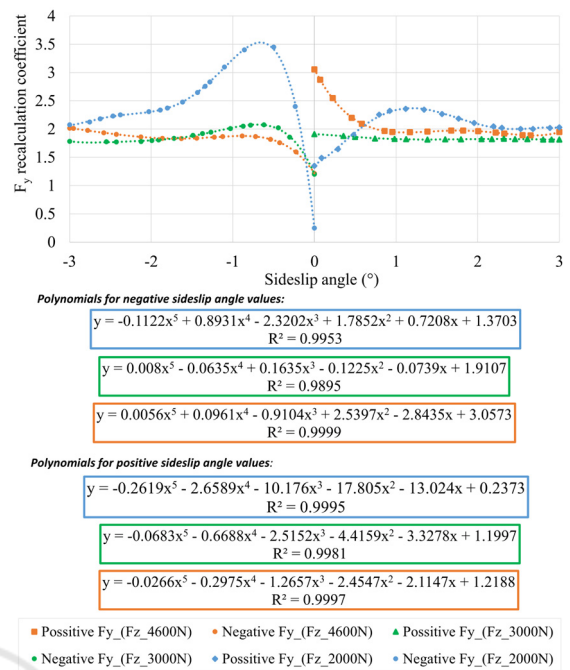


Figure 4: Examples of lateral tyre force recalculation coefficients for few loading cases.

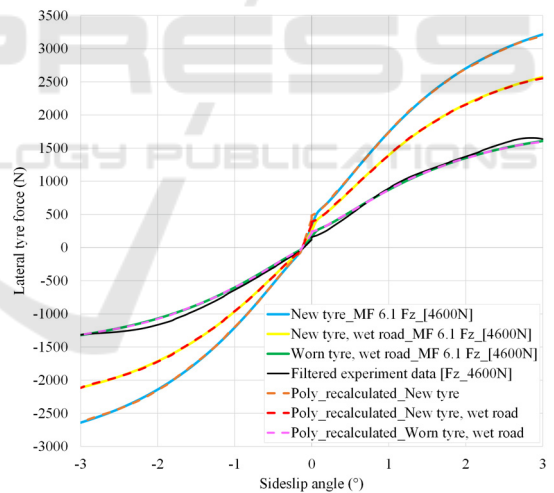


Figure 5: Lateral tyre force recalculation for medium vertical loading scenario (4600 N).

### 3.1 Process of Interpolation

Since vertical load on the test rig is not affected by the roll and pitch dynamics, it may only be changed manually in a range from 2000 N to 9000 N. Therefore, during the measurements, applying the tyre force recalculation algorithm described above, longitudinal and lateral forces at discrete values of

vertical load,  $F_z$  can be performed and stored as a lookup table (LUT) (Table 2). An algorithm to recalculate longitudinal and lateral forces for every  $F_z$  is needed. This is where interpolation becomes necessary.

Table 2: LUT for  $F_x$  and  $F_y$  estimation.

	$F_z$		
	$F_{zmin}$	...	$F_{zmax}$
Slip, $\lambda$	$F_x(\lambda, F_{zmin})$	...	$F_x(\lambda, F_{zmax})$
Toe angle, $\alpha$	$F_y(\alpha, F_{zmin})$	...	$F_y(\alpha, F_{zmax})$

Interpolation operates on two surrounding points from the LUT. For example, consider the following two points in Table 2 (for  $F_x$  estimation):  $F_x(\lambda, F_{zL})$ ,  $F_x(\lambda, F_{zH})$ . Here:  $\lambda$  is the current slip value,  $F_{zL}$  and  $F_{zH}$  are the lower and upper values of the vertical load. The goal is to interpolate the value of  $F_x$  at a desired slip  $\lambda$  and vertical load  $F_z$ . To calculate the interpolated value  $F_x(\lambda, F_z)$ , we linearly interpolate along the  $F_z$ -axis as follows:

$$F_x(\lambda, F_z) = F_x(\lambda, F_{zL}) + \frac{F_x(\lambda, F_{zH}) - F_x(\lambda, F_{zL})}{(F_{zH} - F_{zL})} (F_z - F_{zL}) \quad (1)$$

A similar approach is used to calculate  $F_y$  based on toe angle and vertical load:

$$F_y(\alpha, F_z) = F_y(\alpha, F_{zL}) + \frac{F_y(\alpha, F_{zH}) - F_y(\alpha, F_{zL})}{(F_{zH} - F_{zL})} (F_z - F_{zL}) \quad (2)$$

This method ensures smooth transitions between the points in the LUT. To end with, overall recalculation sequence can be summarised by these steps: 1) generation of the target curves using MF 6.1; 2) extraction of the actual tyre force curves from the experiments; 3) curve division to obtain recalculation coefficients; 4) polynomial curve fit over the coefficients; 5) force recalculation using the appropriate polynomial; 6) estimation of  $F_x$  and  $F_y$  for any given slip, toe and vertical load combination.

## 4 CASE STUDY

After developing a methodology for longitudinal and lateral force recalculation and considering the vertical load changes, the HIL setup was launched, and initial tests were performed.

The Sin with Dwell manoeuvre was selected for the case study to test rear-wheel toe control. Vehicle velocities of 80 and 100 km/h were used. Three cases were analysed: 1) Passive – a vehicle with corners, without toe actuators; 2) Model – a vehicle with corners and toe actuators. Notation "Model" refers to the fact that the request of the mathematical model is fed into the HIL test rig, but the actual position and the response of the HIL is not fed-back into the mathematical model. This means that "Model" is an idealised system running in open loop; 3) HIL – a vehicle with corners and toe actuators realised in closed loop HIL application. Results are presented in Figures 6 and 7.

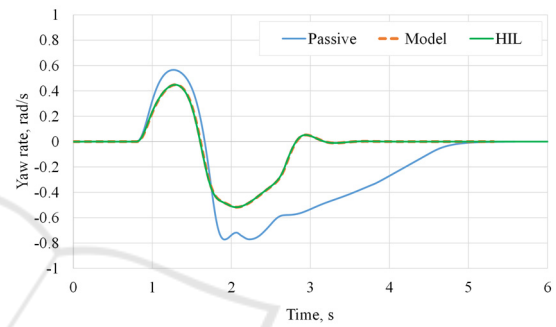


Figure 6: Sin with Dwell at 80 km/h.

The toe actuators installed on HIL at lower vehicle velocities could follow the target angle perfectly. Feeding the actuator's position to the vehicle model in real-time produced no distortions to the yaw rate and overall vehicle response. Figure 6 shows no difference between the Model and HIL results; the RMSE value for this case under investigation is only 0.00438 rad/s. It needs to be mentioned that the passive system could not perform manoeuvres.

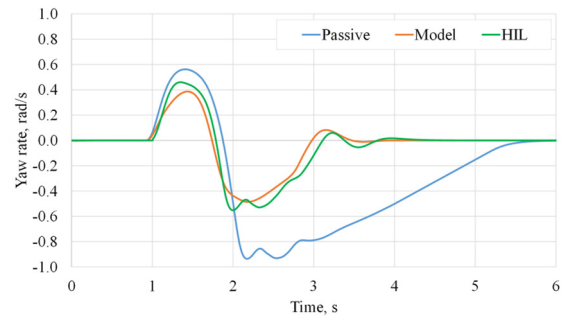


Figure 7: Sin with Dwell at 100 km/h.

However, the difference between the Model and HIL results appears at the higher vehicle speed (100 km/h, Figure 7). After analysing the results, it was found that the toe actuator does not repeat the

reference value so well as in a previous case (Figure 8); RMSE is  $0.55^\circ$  even though the manoeuvre was performed successfully.

Due to the rule-based control strategy used for active toe system, actuator nonlinearity, delay, and fluctuations, the differences are more pronounced. Since the mathematical model does not include any actuator dynamics, it presents an idealised system. Using the HIL simulation with real actuators allows us to fully evaluate the effectiveness of the control system and its influence on the vehicle dynamics.

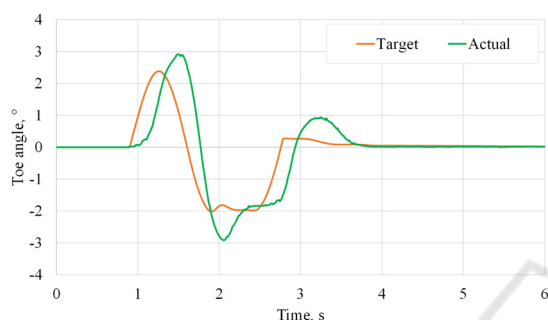


Figure 8: Reference toe and actual toe value at velocity 100 km/h.

HIL experiments show that the actual yaw rate differs from the one in the idealised system. Hence, these outcomes from the HIL application can help further develop the control system, mitigate control errors, and ensure proper vehicle response. However, it will be presented in future works.

## 5 CONCLUSIONS

With the completed investigation, there are several conclusions:

1. A test rig for vehicle corner testing has been manufactured, and a HIL system has been developed. A real-time, high-fidelity mathematical model of the vehicle is utilised within the HIL, with the rear axle corner swapped for physical components.
2. Since the test rig incorporates a vehicle quarter, it cannot accurately account for roll and pitch angles; consequently, the vertical loading does not reflect reality. Additionally, the contact between the tyre and the drum does not adequately represent the actual contact between the tyre and the road surface. Various road types, such as dry and wet asphalt, ice, and other surfaces, cannot be represented effectively. Therefore, a methodology for recalculating longitudinal and lateral forces

has been developed to consider different loading conditions, and the obtained results have been compared with ground truth.

3. A case study demonstrating toe actuator testing is presented. At up to 80 km/h velocities for the selected manoeuvre, the results achieved with HIL and the mathematical model are very similar (with a RMSE of  $0.0048$  rad/s). However, as the velocity increases, discrepancies arise due to the nonlinearity of actuator and noise from the sensors, which is not addressed within the mathematical model.
4. Using the HIL approach, it was found that active toe control of a vehicle equipped with corners improves its dynamics. A vehicle with passive corners, which includes IWM but does not contain an active toe control system, is not able to perform Sin with Dwell manoeuvre even at 80 km/h.
5. Finally, further modifications to the control algorithm are necessary. The case study demonstrated the advantages of employing HIL for investigations. However, control algorithms are not the primary focus of this paper and will be explored in future work.

## ACKNOWLEDGEMENTS

This work was supported by the Research Council of Lithuania project no. S-MIP-23-120.

## REFERENCES

- Armengaud, E., Eitzinger, S., Pirker, H., Buh, J., Gramstat, S., Heimann, S., Chen, C., Ivanov, V., Heydrich, M., Sorniotti, A., Gruber, P., and Tavernini, D. (2021). E-Mobility-Opportunities and Challenges of Integrated corner Solutions. *SAE International Journal of Advances and Current Practices in Mobility*, 3(5), 2462–2472. <https://doi.org/10.4271/2021-01-0984>
- Arosio, D., Braghin, F., Cheli, F., and Sabbioni, E. (2005). Identification of Pacejka's scaling factors from full-scale experimental tests. *Vehicle System Dynamics*, 43(sup1), 457–474. <https://doi.org/10.1080/00423110.500229683>
- Augsburg, K., Gramstat, S., Horn, R., Ivanov, V., Sachse, H., and Shyrokau, B. (2011). Investigation of brake control using Test Rig-in-the-Loop technique. *SAE Technical Papers on CD-ROM/SAE Technical Paper Series*. <https://doi.org/10.4271/2011-01-2372>
- Cheng, S., Peng, H.-N., Yang, C., Wang, W.-D., and Li, L. (2024). Chassis Global Dynamics Optimization for Automated Vehicles: A Multiactuator Integrated Control Method. In *IEEE Transactions on Systems*,

- Man, and Cybernetics: Systems*, 54(1), pp. 578–587. <https://doi.org/10.1109/tsmc.2023.3311446>
- Chindamo, D., Gadola, M., and Marchesin, F. P. (2017). Reproduction of real-world road profiles on a four-poster rig for indoor vehicle chassis and suspension durability testing. *Advances in Mechanical Engineering/Advances in Mechanical Engineering*, 9(8), 168781401772600. <https://doi.org/10.1177/1687814017726004>
- Deepak, K., Frikha, M. A., Benômar, Y., Baghdadi, M. E., and Hegazy, O. (2023). In-Wheel motor drive systems for electric vehicles: state of the art, challenges, and future trends. *Energies*, 16(7), 3121. <https://doi.org/10.3390/en16073121>
- Fathy, H. K., Filipi, Z. S., Hagen, J., and Stein, J. L. (2006). Review of hardware-in-the-loop simulation and its prospects in the automotive area. *SPIE Proceedings*. <https://doi.org/10.1117/12.667794>
- Gießler, Martin, Gauterin, F., & and Unrau, H. J. (2022). New inner drum test bench for dynamic tests of PLT and truck tires. KITopen-ID:1000156885. <https://doi.org/10.5445/IR/1000156885>
- Gräbe, R. P., Kat, C., Van Staden, P. J., and& Els, P. S. (2020). Difference thresholds for a vehicle on a 4-poster test rig. *Applied Ergonomics/Applied Ergonomics*, 87, 103115. <https://doi.org/10.1016/j.apergo.2020.103115>
- Guo, L., Ge, P., and& Sun, D. (2019). Torque Distribution Algorithm for stability control of electric vehicle driven by four In-Wheel motors under emergency conditions. *IEEE Access*, 7, 104737–104748. <https://doi.org/10.1109/access.2019.2931505>
- Gysen, B., Paulides, J., Janssen, J., and& Lomonova, E. (2010). Active electromagnetic suspension system for improved vehicle dynamics. *IEEE Transactions on Vehicular Technology*, 59(3), 1156–1163. <https://doi.org/10.1109/tvt.2009.2038706>
- Heydrich, M., Ivanov, V., Bertagna, A., Rossi, A., Mazzoni, M., and& Büchner, F. (2022). Hardware-in-the-Loop testing of a hybrid Brake-by-Wire system for electric vehicles. *SAE International Journal of Vehicle Dynamics, Stability, and NVH*, 6(4). <https://doi.org/10.4271/10-06-04-0031>
- Hori, Y. (2004). Future Vehicle Driven by Electricity and Control—Research on Four-Wheel-Motored "UOT Electric March II." *IEEE Transactions on Industrial Electronics*, 51(5), 954–962. <https://doi.org/10.1109/tie.2004.834944>
- Ivanov, V., Augsburg, K., Bernad, C., Dhaens, M., Dutré, M., Gramstat, S., Magnin, P., Schreiber, V., Skrt, U., and& Van Kelecom, N. (2019). Connected and shared X-in-the-Loop technologies for electric vehicle design. *World Electric Vehicle Journal*, 10(4), 83. <https://doi.org/10.3390/wevj10040083>
- Jneid, M. S., and& Harth, P. (2024). Radial Flux In-Wheel-Motors for vehicle electrification. *Cognitive Sustainability*, 3(3). <https://doi.org/10.55343/cogsust.105>
- Kojis, P., Danilevičius, A., Šabanovič, E., and& Skrickij, V. (2022). The second generation of electric vehicles: Integrated Corner Solutions. In Lecture notes in intelligent transportation and infrastructure (pp. 87–100). [https://doi.org/10.1007/978-3-030-94774-3\\_9](https://doi.org/10.1007/978-3-030-94774-3_9)
- Lauwerys, C., Swevers, J., and& Sas, P. (2005). Robust linear control of an active suspension on a quarter car test-rig. *Control Engineering Practice*, 13(5), 577–586. <https://doi.org/10.1016/j.conengprac.2004.04.018>
- Li, I., and& Lee, L. (2019). Design and development of an active suspension system using Pneumatic-Muscle actuator and intelligent control. *Applied Sciences*, 9(20), 4453. <https://doi.org/10.3390/app9204453>
- Maher, D., and& Young, P. (2010). An insight into linear quarter car model accuracy. *Vehicle System Dynamics/Vehicle System Dynamics*, 49(3), 463–480. <https://doi.org/10.1080/00423111003631946>
- Mihalič, F., Truntič, M., and& Hren, A. (2022). Hardware-in-the-Loop Simulations: A Historical Overview of Engineering Challenges. *Electronics*, 11(15), 2462. <https://doi.org/10.3390/electronics11152462>
- Nguyen, B.-M., and& Trovão, J. P. (2024). Advancing Automotive Electronics: The Role of Collaborative Education and Project Development [Automotive Electronics]. *IEEE Vehicular Technology Magazine*, 19(3), pp. 116–127. <https://doi.org/10.1109/mvt.2024.3414068>
- Omar, M., El-Kassaby, M., and& Abdelghaffar, W. (2017). A universal suspension test rig for electrohydraulic active and passive automotive suspension system. *Alexandria Engineering Journal /Alexandria Engineering Journal*, 56(4), 359–370. <https://doi.org/10.1016/j.aej.2017.01.024>
- Šabanovič, E., Kojis, P., Šukevičius, Š., Shyrokau, B., Ivanov, V., Dhaens, M., and& Skrickij, V. (2021). Feasibility of a neural Network-Based virtual sensor for vehicle unsprung mass relative velocity estimation. *Sensors*, 21(21), 7139. <https://doi.org/10.3390/s21217139>
- Skrickij, V., Kojis, P., Šabanovič, E., Shyrokau, B., and& Ivanov, V. (2024). Review of Integrated chassis control techniques for Automated ground vehicles. *Sensors*, 24(2), 600. <https://doi.org/10.3390/s24020600>
- Society of Automotive Engineers International. (2012). Laboratory Testing Machines for Measuring the Steady State Force And Moment Properties of Passenger Car Tires (SAE J 1106). [https://doi.org/10.4271/J1106\\_201208](https://doi.org/10.4271/J1106_201208)
- Stolte, T., Loba, M., Nee, M., Wu, L., and& Maurer, M. (2023). Toward Fault-Tolerant Vehicle Motion Control for Over-Actuated Automated Vehicles: A Non-Linear Model Predictive Approach. *IEEE Access*, 11, 10499–10519. <https://doi.org/10.1109/access.2023.3239518>
- Yu, M., Arana, C., Evangelou, S. A., and& Dini, D. (2019). Quarter-Car Experimental Study for Series Active Variable Geometry Suspension. *IEEE Transactions on Control Systems Technology*, 27(2), 743–759. <https://doi.org/10.1109/tcst.2017.2772912>